Available online at www.sciencedirect.com
SCIENCE DIRECT®
Microelectronic Engineering 83 (2006) 476–484
MICROELECTRONIC ENGINEERING
www.elsevier.com/locate/mee

# Experimental test chamber design for optics exposure testing and debris characterization of a xenon discharge produced plasma source for extreme ultraviolet lithography

Keith C. Thompson *, Erik L. Antonsen, Matthew R. Hendricks, Brian E. Jurczyk, M. Williams, D.N. Ruzic

*Department of Nuclear, Plasma, and Radiological Engineering, Plasma-Material Interaction Group, University of Illinois at Urbana-Champaign, 103 S. Goodwin Avenue, 214 NEL, Urbana, IL 61801, USA*

Received 2 August 2005; received in revised form 16 November 2005; accepted 16 November 2005
Available online 12 December 2005

**Abstract**

A commercial EUV light source is currently used in the MS-13 EUV Micro Exposure Tool (MET) produced by Exitech Ltd. The source uses a xenon z-pinch discharge to produce 13.5 nm light intended for use in extreme ultraviolet lithography (EUVL). During operation, an erosive flux of particles is ejected from the pinch plasma, contributing to limitations in the lifetime of nearby collector optics. A diagnostic chamber is presented that permits characterization of the debris fields present, exposure of optical samples, and evaluation of debris mitigation techniques. Available diagnostics include a Faraday cup, a spherical sector energy analyzer (ESA), and a EUV photodiode. This paper details the chamber design and initial results of source characterization. Faraday cup analysis shows that the maximum theoretical ion energy is 53 keV, ESA measurements show the presence of $Xe^{+}$, $Xe^{2+}$, $Ar^{+}$, $W^{+}$, and $Mo^{+}$ ions, and microanalysis of exposed mirror samples is used to show the erosive effects of plasma exposure.


*Keywords:* Extreme ultraviolet; Microlithography; Debris mitigation; Plasma; z-Pinch

## 1. Introduction

Extreme ultraviolet lithography (EUVL) is currently under development by the semiconductor industry as a candidate technology for high-volume manufacturing (HVM) of integrated circuits (ICs) at and below the 32 nm node. The EUV LLC (Extreme Ultraviolet Limited Liability Corporation) Consortium, founded by Intel, Motorola, and AMD, selected the 13.5 nm (originally 13.4 nm) extreme ultraviolet (EUV) wavelength for research in the 1990s. Experiments were done by 2002 that successfully demonstrated scanned printing of sub 100 nm features [1], triggering industry acceptance of EUV as the leading "Next Generation Lithography" (NGL).

There are two source technologies competing for application to high-volume manufacturing of ICs. The first is laser produced plasmas (LPP) that create highly charged ions by focusing a pulsed laser on a liquid fuel target [2]. The experiments done here use the second type, a discharge produced plasma (DPP) that uses xenon gas in a z-pinch discharge [2].

For extreme ultraviolet lithography, large collector optics must be located a short distance from the dense plasma pinch. These specialized mirror assemblies consist of thin films and can be either specialized multilayer mirrors (MLMs) for near normal incidence reflection or single layers for grazing incidence reflection. These apparatus collect and focus the EUV light for use in lithography. Over time, the proximity to the pinch plasma results in surface degradation due to an erosive flux of ions and neutral particles ejected from the plasma column. Unscattered heavy

* Corresponding author. Tel.: +1 217 333 6291; fax: +1 217 333 2906.
*E-mail address:* kcthmpsn@uiuc.edu (K.C. Thompson).

0167-9317/$ - see front matter © 2005 Elsevier B.V. All rights reserved.
doi:10.1016/j.mee.2005.11.012

ions and neutrals on a direct vector from the source are suspected to be the primary cause of surface erosion within the chamber. Damage is also caused by scattered ions and neutral particles that have lost energy through collisions. For HVM viability, source power and optics lifetime increases of 10–1000 times are necessary. Significant effort is currently being expended to mitigate the source debris problem and extend collector optics lifetime for both LPP and DPP sources at current and future power levels.

The XTREME [3] Commercial EUV Emission Diagnostic (XCEED) experimental test chamber is designed to facilitate characterization of the source plasma and the debris fields emitted by the DPP, along with optical sample exposure to the pinch plasma. This paper discusses the XCEED chamber design and characterization of the DPP source. Efforts are directed towards characterizing fast ion debris, exploring the erosive effects on mirror surfaces, evaluating debris mitigation techniques, and developing novel methods to mitigate damage to collector mirrors. In Section 2, the custom experimental chamber is discussed and its capabilities are examined. Experiments are outlined for evaluating EUV output, exploring mirror reflectivity degradation, taking Faraday cup measurements, and characterizing ion debris using a spherical sector energy analyzer (ESA). Methods for optical sample exposure are discussed along with techniques for assessing erosive effects. Experimental results of photodiode measurements of EUV output, Faraday cup analysis of the ion debris, and ESA analysis of fast ion species are presented and discussed in Section 3. Conclusions are drawn in Section 4.

## 2. Apparatus and approach

### 2.1. EUV light source and debris mitigation tool

The XTREME Technologies XTS 13-35 [3] is a DPP source currently used in the Exitech Ltd. Micro Exposure Tool (MET). This plasma source uses xenon gas to create 35 W of EUV light (2% bandwidth) in $2\pi$ sr with a conversion efficiency of 0.55%. The self-compression of the Xe gas column results in heating sufficient for the generation of $Xe^{8+}$ to $Xe^{12+}$ ions, necessary for the emission of EUV light at 13.5 nm. The source as configured at UIUC is capable of operating at continuous pulse rates of 1 kHz and in "burst" mode up to 2 kHz. In addition to XTREME, several other groups are competing in the field of DPP EUV source development, including Cymer Inc., Philips Inc., and PLEX LLC. A comparison of their best efforts reported at the Third International EUVL Symposium in November of 2004 is given in Table 1.

There are several innovations represented in the XTREME tool compared to typical laboratory z-pinch experiments at these power levels. It is capable of the high-repetition rate without melting of the electrodes due to porous metal cooling [2]. Also, it utilizes saturable-core inductors in the charging circuit to deliver a very fast voltage rise-time and a recharge-circuit that allows full utilization of the electrical input energy. The pre-ionization technique is also unique [9].

The manufacturer has provided a foil trap-based [10] debris mitigation tool to explore methods of reducing particle transfer from the pinch to collector optics. A foil trap is designed similar to a collimator (as used in CVD/PVD processes), with flat pieces of metal placed with their planar normal direction perpendicular to the path of light from the pinch. They are positioned radially and in such a way as to obscure the minimum amount of light from the pinch as illustrated in Fig. 1. Ideally, particles are scattered by the background gas and extinguished against the walls of the foil trap, thus failing to traverse to the optics further inside

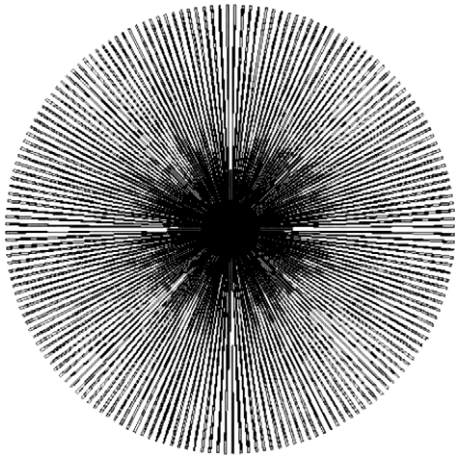

Fig. 1. Illustration of the foil trap concept as seen from the pinch plasma.

Table 1
Comparison of best reported efforts in xenon DPP EUV source technology [4–7]

| Source maker | Cymer | Philips | XTREME | PLEX LLC |
|---|---|---|---|---|
| Source type | DPP | DPP | DPP | DPP |
| Source fuel | Xenon | Xenon | Xenon | Xenon |
| Continuous operating frequency | 2.5 kHz | N/A | 1 kHz | 6 kHz |
| EUV output power, $2\pi$ sr | 140 W | 120 W | 200 W | 100 W |
| Conversion efficiency | 0.45% | 0.50%[a] | 1.00% | 0.50% |
| Measured ion spectra | No data[b] | No data[b] | Published[c] | No data[b] |

[a] Extrapolated data.
[b] No data have been published or otherwise publicly disclosed.
[c] See Ref. [8].

the chamber. An argon gas curtain is added to provide an enhanced scattering possibility for particles ejected from the plasma. The gas curtain is an area of gas pressure greater than that near the pinch or in the main chamber. The density of the gas curtain is controlled through the manipulation of the buffer gas flow rate and chamber pumping speeds.

### 2.2. Experimental chamber description

The XCEED experimental chamber is shown in Fig. 2. It was manufactured to specifications by Kurt J. Lesker Co. [11] and consists of a short cylinder made of 304L stainless steel, 36-in. in diameter and 14-in. tall with one end domed. The flat end mates to the XTS 13-35 source by means of a custom designed adapter flange. The domed end and sides accommodate all of the diagnostics, vacuum pumps, and other ports. Chamber connection to the plasma source is illustrated with emphasis on direct field-of-view measurement capability from seven ports focused on the z-pinch. Separated by 5°, these ports cover 15–45° from the centerline of the chamber. These provide the means to characterize the angular spread of source light output and ejecta. Diagnostics mounted on these ports include a Faraday cup, EUV photodiode, and a spherical sector electrostatic energy analyzer. There are 15 ports used for sample manipulation, discussed below. Separate ports house a residual gas analyzer (RGA) and power feedthroughs for a radio frequency plasma coil. Three ISO 250 ports are available for pump connections. The chamber is evacuated by two Osaka TG-M series compound molecular pumps backed by an Ebara Model 80X25 UERRGM Dry Pump. Base pressures achieved are on the order of $10^{-7}$ Torr, which is similar to the level of vacuum achieved by the XTS 13-35 in the field.

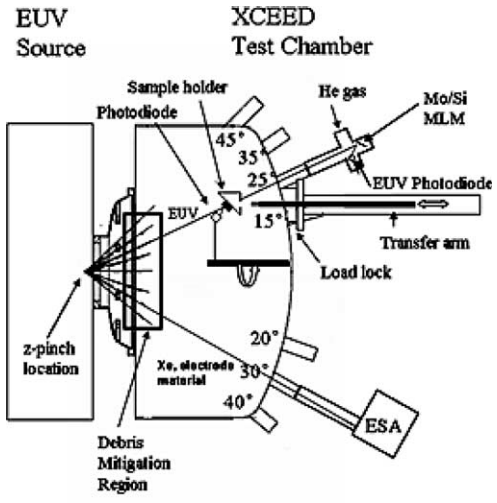


Fig. 2. Diagram showing the interface of the XTS 13-35 Commercial EUV light source and the UIUC XCEED test chamber.

There are four sample locations within the chamber. Each has a mounting port, load-lock extraction port, viewing window, and thermocouple feedthrough for temperature measurement. The load-lock apparatus allows samples to be removed during tests at varying exposure durations without disturbing the remaining samples. This is critical to minimizing transient effects that are caused by electrode thermal cycling from discontinuous source operation. Fig. 3 shows a schematic view of sample manipulation by the load-lock. A single load-lock apparatus can be moved among the four sample positions to remove samples for analysis during testing.

The sample holder apparatus are custom designed aluminum blocks with indentations for mirror sample positioning. Samples are attached with carbon tape to the sample holders and positioned to present the samples to the light source at either a 23° (grazing) or 80° (normal) incidence angle. This configuration is shown in Fig. 4. Sample reflectivity can be assessed in situ through shielded photodiodes for both normal and grazing configurations. Measurements of relative changes in reflectivity are obtained by comparison of the in situ photodiode output with measurements from the control photodiode. The photodiodes are discussed in more detail below.

As samples are removed from the chamber during exposure testing, microanalysis of roughness changes and element implantation are performed for a time-dependent illustration of sample degradation through exposure. Microanalysis experiments include measurements of roughness changes, erosion, texture, and composition through the use of atomic force microscopy (AFM),

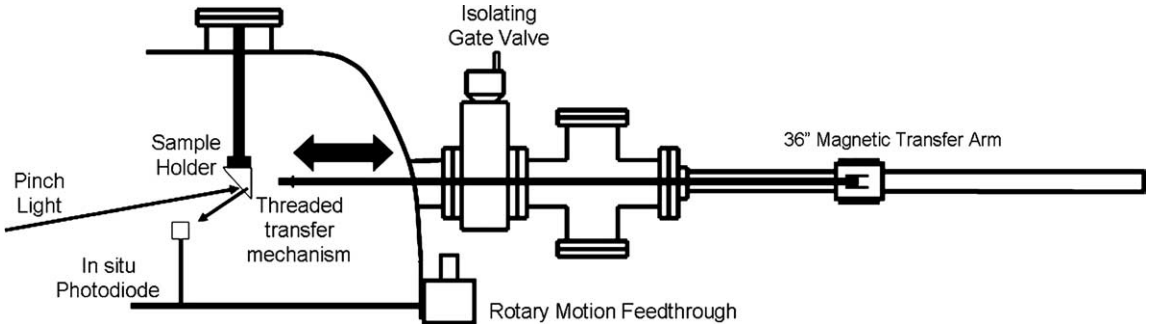


Fig. 3. Optical samples in chamber are removed through a load-lock without turning off the source.

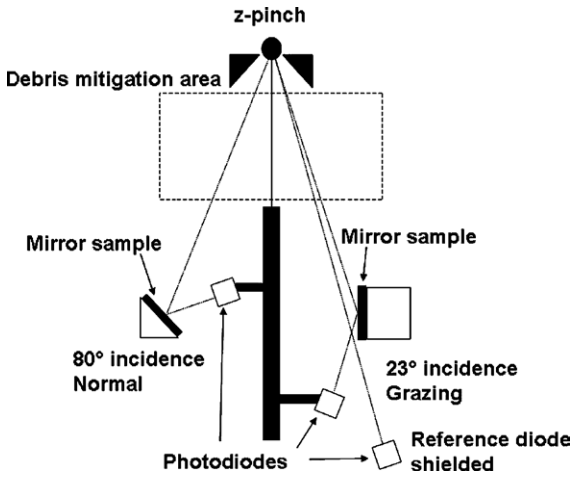


Fig. 4. Schematic of sample exposure setup and working process.

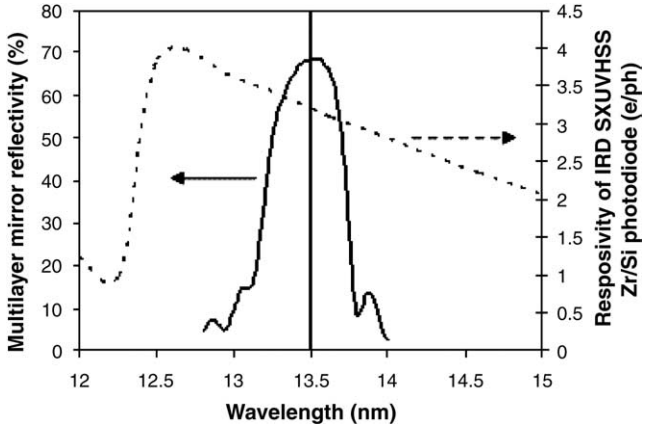


Fig. 6. Selectivity of multilayer mirror [18] and IRD photodiodes used in control photodiode assembly.

X-ray reflectivity (XRR), X-ray diffraction (XRD), Auger electron spectroscopy (AES), X-ray photoelectron spectroscopy (XPS), and scanning electron microscopy (SEM). These experiments are detailed elsewhere [12], but results are referenced here.

### 2.3. EUV photodiode

EUV output from the source is measured using International Radiation Detectors (IRD) [13] SXUVHS5 Zr/Si EUV photodiodes. The reference photodiode is mounted external to the chamber on an angled port in a single bounce configuration using a specialized Mo/Si multilayer mirror that provides in-band selectivity for EUV light measurements. There is a 2-mm orifice limiting particle flux and the assembly is back-filled with Helium gas to mitigate damage to the mirror. This assembly, shown in Fig. 5, monitors EUV output during debris characterization and provides a control reference during in situ reflectometry measurements on exposed mirror samples. The photodiode is placed such that the reflected light is incident on the 1-$mm^2$ active surface. The diodes used also have built-in

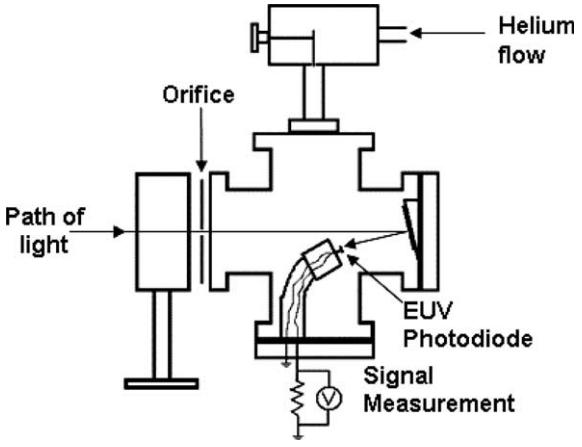


Fig. 5. Diagram of the control photodiode assembly.

Zr/Si filters which block relatively long wavelengths that the multilayer mirror reflects. The EUV selectivity is governed by the reflectivity of the multilayer mirror combined with the responsivity of the filtered photodiode as shown in Fig. 6. The resulting bandwidth is approximately 4%.

Two International Radiation Detectors SXUVHS5 Zr/Si EUV photodiodes are placed inside the main chamber for in situ measurements of the surface reflectivity of mirror samples as they are exposed over time. They are shielded from direct debris impact, but are subject to damage from reflected particles in the chamber. These photodiodes measure light reflected from mirror samples mounted in the chamber at normal and grazing light incidences. The in situ photodiodes are affixed to the shaft of a Kurt J. Lesker Company Model KZRD275037HS motorized rotary feedthrough, and can be rotated to measure reflected light from any of the four sample locations within the chamber.

### 2.4. Faraday cup

A Comstock [14] model FC610 Faraday cup is mounted inside a 4.5 in. CF vacuum nipple, with electrical isolation provided by a solid piece of unfired Alumina. Two stainless steel mesh screens are placed approximately 0.7 in. and 1.3 in. in front of the Faraday cup to isolate it from residual plasma inside the main chamber.

The Faraday cup signal is generated by the impingement of three different types of particles: photons, electrons, and ions. When the z-pinch occurs, it emits light from electron excitation and decay along with free electrons and ions. Photons impinge on the surface of the Faraday cup first and transfer their energy to the metal. In doing so, they free electrons from the surface through the photoelectric effect. This loss of electrons causes an initial positive signal to be measured on the oscilloscope. While the Faraday cup is designed to recapture these electrons, it does not do so without error. In this experiment, the rim of the cup is directly exposed to pinch debris such that electrons released from the metal in this area are generally not recaptured.

Since electrons are 1836 times lighter than the smallest ion and subject to the same electromotive force, the electrons from the pinch reach the Faraday cup next. This new abundance of negative charges causes a downward peak on the oscilloscope that follows the photoelectric peak. Ions colliding with the surface after this cause a positive signal that lasts for an amount of time related to the energy distribution and mass of the ions. Ion energy distribution can be determined from this through time-of-flight analysis if the ion species and charge states are known. The equation relating time of arrival and energy is given by

$$E\ (\mathrm{eV}) = \left(\frac{m}{2}\right)\left(\frac{d^2}{t^2}\right)\left(\frac{1}{1.6022\times 10^{-19}}\right) \quad (1)$$

where $E$ is ion energy (eV), $m$ is particle mass (kg), $d$ is the distance traversed by the ions (m), and $t$ is the ion time of flight (s). The Faraday cup is located 0.88 m from the pinch and, if it is assumed that the impinging ions are predominantly xenon, the ion energy distribution can be determined. The time constant associated with the Faraday cup and the attached circuitry results in a settling time that does not allow for differentiation between the tail end of the electron signal and the leading edge of the ion signal. Therefore, the electrons must be filtered before they reach the diagnostic.

Filtering is accomplished by placing a magnetic field across the path of the measured particles. This allows electrons to be diverted away from the Faraday cup while the path of the heavier ions is negligibly affected. The percentage of electrons diverted depends on their energy distribution and the strength of the field, as the force on the particles is given by

$$F = qB\sqrt{\frac{2E}{m}} \quad (2)$$

where $q$ is the elementary charge, $m$ is the mass of the particle, $E$ is energy, and $B$ is the strength of the magnetic field. The field strength is selected such that loss of electrons due to photon impingement is equilibrated by the arrival of pinch electrons. This allows the ion signal to be measured from an effective zero-volt baseline. Furthermore, the chamber gas pressure affects the energy distribution of electrons reaching the Faraday cup due to electron-neutral collisions. This affects the requirement for magnetic field strength.

Four different magnet strengths are used with two different chamber gas pressures for a total of eight experimental conditions. Magnetic fields of 0.0, 10.6, 38.8, and 48.8 mT are tested with chamber pressures of 0.9 and 11.4 mTorr.

### 2.5. Spherical sector energy analyzer

A Comstock AC-902B Spherical Sector Energy Analyzer is fitted with a set of Burle [15] dual microchannel plates (MCP) to measure the flux of ion debris emitted by the plasma source [8]. The analyzer has direct line-of-sight access to the source through seven 2.75 in. CF ports positioned at angular intervals of 5° from 15° to 45° off of the centerline of the pinch. Access at the centerline is impeded by the beam stop of the debris tool. The ESA is connected to the chamber through a vacuum bellows to allow for 3-dimensional positioning. A 1 mm orifice is placed after the bellows for differential pumping to satisfy the low pressure requirement of the ESA.

The ESA consists of two spherical segments that are charged to equal and opposite voltages to guide ions of a specific energy-to-charge ratio between them towards the MCPs. Ions with too much energy extinguish against the outer wall, while ions with too little energy extinguish against the inner wall. Neutral and negatively charged particles are also unable to traverse the spherical path.

The first microchannel plate amplifies the secondary electron emission from the collision of a single particle by means of an electron cascade through an individual microchannel. The second MCP further amplifies the signal using the electrons generated by the first MCP to initiate numerous more electron cascades. The electrons then collect on a metal plate to create a signal with a pulse width of less than $10^{-8}$ s.

## 3. Results and discussion

### 3.1. Photodiode

The response of the control photodiode to the light emitted during a single pinch is a narrow positive peak (Fig. 7). The pulse width is less than 2 μs and the peak generally varies around 4.5 mV. Integrating this area provides a value for the total energy of EUV light emitted in V s. This can be directly converted to a value in traditional units if the reflectivity of the single bounce mirror and the characteristic response of the photodiode are accurately known. For the purposes of this paper, such a conversion is not necessary and is not completed.

Ideally, the control photodiode maintains consistent measurement ability for the plasma source due to its protection from the ion flux, independent of exposure time.

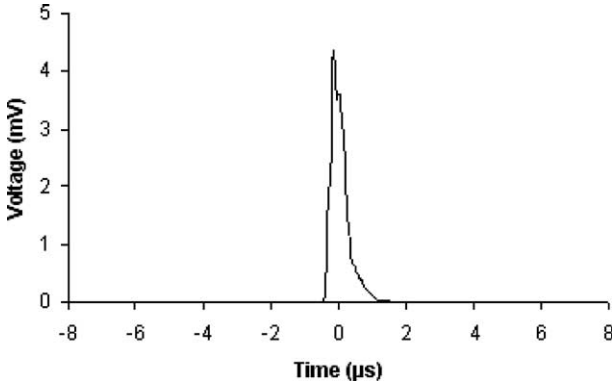


Fig. 7. Typical raw signal obtained from the UIUC XCEED control photodiode assembly excited by the EUV output of the XTS 13-35 z-pinch source.

Practical application of the measurement technique, however, results in damage to both the reflecting mirror and photodiode surface. Design and application techniques are intended to minimize signal degradation, however. Fig. 8 shows the area of the photodiode signal as it varies with pinch frequency. While the EUV output peaks slightly at 2 Hz, it varies by no more than 3.5% from the average value over the evaluated range. Pinch frequencies above 64 Hz are not explored. This is not surprising, however, considering the rate of flow of xenon into the chamber. Xenon at room temperature has a thermal velocity of 220 m/s, so the approximate amount of time it takes for the xenon supply to traverse the length of the pinch compression region (~1–2 cm) is 91 μs. This corresponds to a xenon replenishment frequency of ~11 kHz which is significantly greater than the pinch frequencies considered here. Fig. 9 shows that the addition of buffer gas into the system has a negative impact on the level of EUV output. At the maximum rate of buffer gas flow used in these experiments, the EUV output signal is reduced by 46% at a distance of 0.95 m from the source.

While the reduction in debris due to the gas curtain debris mitigation [8] is beneficial in that it increases the life of nearby collector optics, the decrease in EUV output power is a shortcoming that must be considered in turn. In order to have a viable product, EUV source suppliers must meet the EUV output power requirements determined by collector efficiencies along with the provisions established by the best efforts of photoresist suppliers. A goal of 115 W at the intermediate focus is currently set [16], while source suppliers' best efforts reported during the 3rd International EUVL Symposium in Miyazaki, Japan in November of 2004 fell short by ~50%. However, the values reported were on the order of one magnitude higher than the efforts reported two years before, so there is confidence that the power requirement can be met in time. The need for both effective debris mitigation and sufficient EUV output power is critical to the effort towards EUV lithography in high volume manufacturing. Fortunately, the ambient gas pressure inside the main chamber is a side effect of the gas used for debris mitigation. Increasing the pumping speed behind the DMT would decrease the amount of gas present in the main chamber and thus would decrease the level of EUV light absorption. While scattering inside the main chamber also contributes to the level of debris mitigation observed, it is believed that the majority of particle scattering occurs inside of the DMT. Furthermore, it should be noted that the XCEED test chamber and overall pumping capabilities do not necessarily match the conditions used in the field.

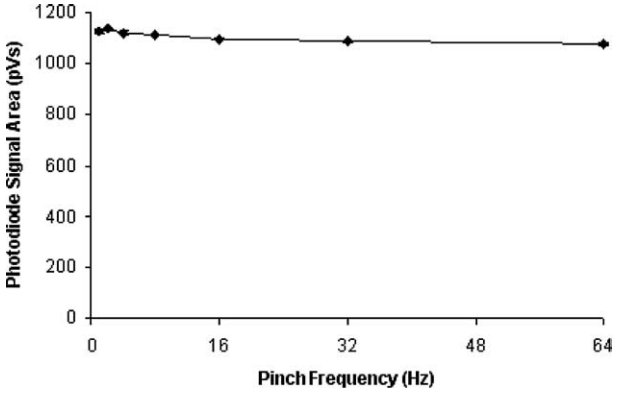


Fig. 8. Integral of the photodiode signal magnitude vs. pinch frequency with no buffer gas.

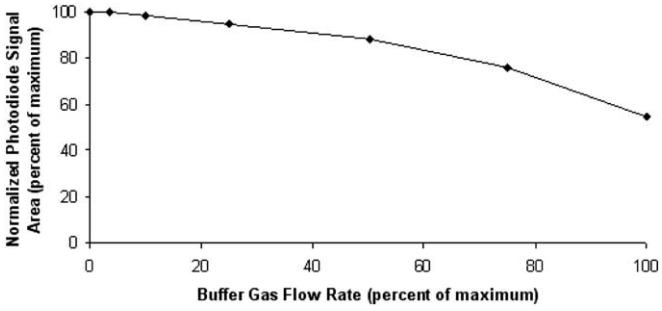


Fig. 9. Integral of the photodiode signal magnitude vs. Ar flow rate at 64 Hz pinch frequency.

### 3.2. Faraday cup ion signal

The initial positive signal from electrons lost through the photoelectric effect can be seen in Fig. 10. Effects of magnetic filtering on the Faraday cup signal are shown in Fig. 11. The signal with no magnetic filtering is distinguished by its large negative spike. As the strength of the field is increased, more electrons are diverted and the signal becomes increasingly positive due to lack of compensation for photoelectron loss.

In one case, the magnetic filtering successfully neutralizes the photoelectron charge loss, and the signal reaches zero before ion impingement begins. This case is shown in Fig. 12, with a magnet strength of 38.8 mT in the ion

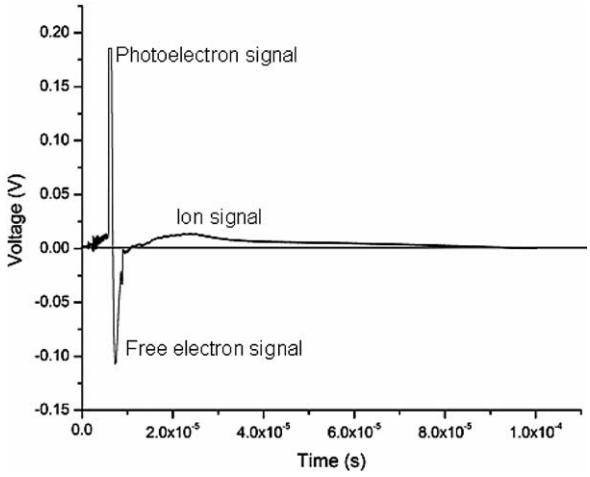


Fig. 10. Faraday cup signal with 8.5 mTorr ambient pressure and no magnetic filtering.

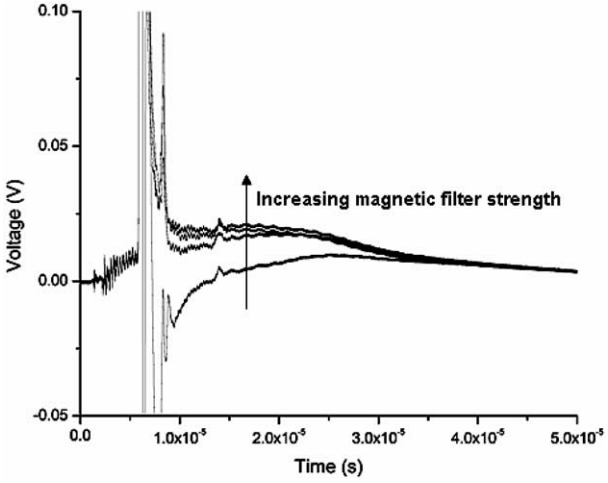


Fig. 11. Faraday cup signals for four different magnetic filtering strengths (including 0 T).

flight path and a chamber pressure of 8.5 mTorr of argon and xenon gasses.

The ion energy distribution can be obtained using Eq. (1). For several ion species that are shown to be present by the ESA, the energy distribution is calculated assuming that the entire ion signal is due only to that species. These plots are normalized to facilitate easy comparison and presented in Fig. 13. Interpretation is best illustrated by an example: if xenon is assumed to be the only ion present, the result suggests that ions are present at energies up to 32 keV. In practice, there exists a dynamic mixture of ions that changes with energy. Without knowing the properties of this mixture as it varies with energy and gas pressure, it is impossible to create an accurate ion energy distribution. Examination of Fig. 13 yields the observation that the largest quantities of ions have energies less than 5 keV. The maximum theoretical energy of each incoming ion species is given by the crossing of the horizontal axis in each corresponding plot.

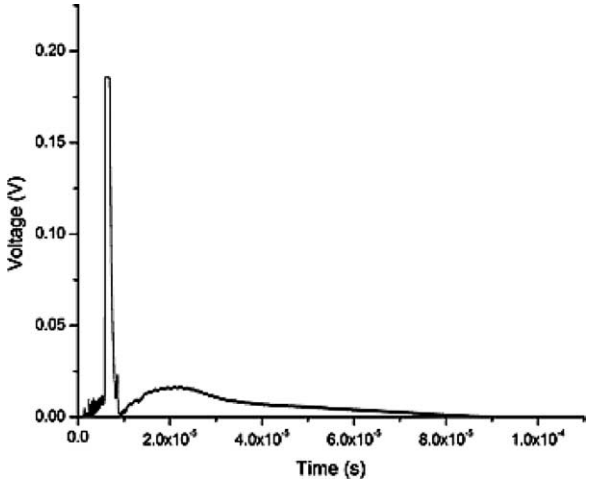


Fig. 12. Faraday cup signal showing proper photoelectron/fast electron charge balance through magnetic filtering.

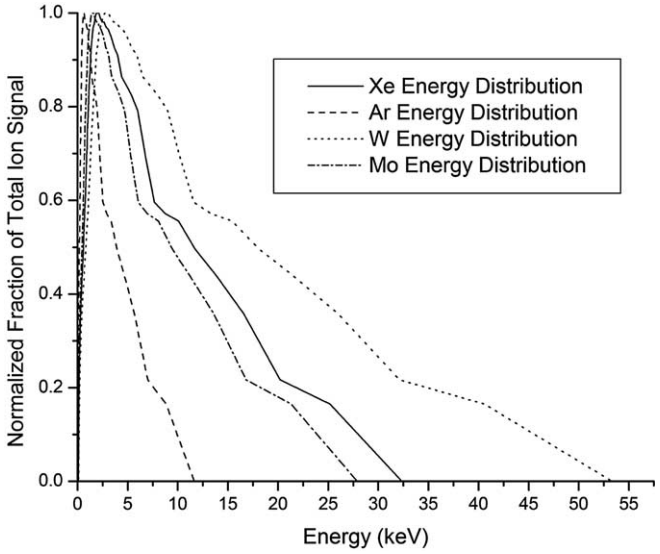


Fig. 13. Ion energy distributions derived from the magnetically filtered Faraday cup signal for different ion specie.

Data from the time-of-flight energy sector analyzer (TOF-ESA) measurements [8] give some insight into the nature of this dynamic mixture of ions. While the ion abundance is thoroughly dominated by $Xe^{+}$ and $Xe^{2+}$, the existence of high energy $Ar^{+}$ and $Mo^{+}$ could account for the initial signal and bring the actual maximum ion energy to under 20 keV. Nonetheless, a Faraday cup alone provides little information when dealing with an ion flux that is made up of multiple elements. Combined with a detailed analysis from an ESA, the data from a Faraday cup signal could be resolved into an ion energy distribution. This would be redundant, however, and would only serve to support the data obtained from the TOF/ESA in the first place.

### 3.3. Optical sample exposures

An experiment is done in which the plasma source is run for 2 h at 256 Hz with a sample holder placed inside. The temperature of the incident surface is measured using a K-type thermocouple attached to the surface with carbon tape. As seen in Fig. 14, the temperature of the sample holders increases to around 110 °C before appearing to level off below the limit of 130 °C recommended by the tape manufacturer, SPI Supplies [17]. This experiment is done without any buffer gas debris mitigation, however. During exposure testing, sample holder temperature is observed to peak at 73 °C, though a comparable surface temperature measurement is not available.

Initial exposure testing of optic samples is an 11-h test in which samples are exposed in the normal orientation (surface is 80° to incoming light vector) as well as the grazing orientation (23° to incoming light vector), and removed from the chamber for microanalysis after 10 million pulses. A set of unexposed samples is analyzed for comparison. Optical samples include six single layer films: Au, C, Mo,

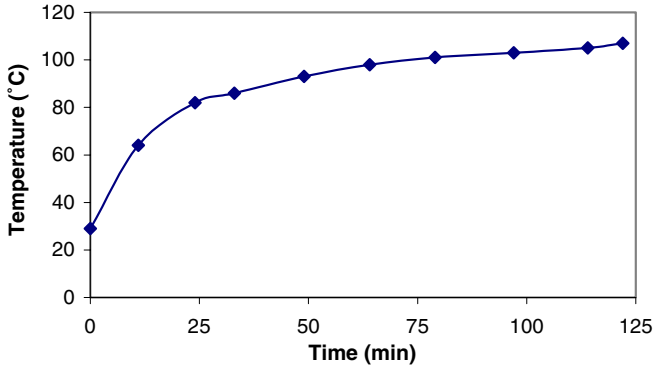


Fig. 14. Sample holder incident surface temperature over time.

Pd, Ru and Si. Also exposed is a Mo/Si multilayer mirror with a Ru capping layer called "ML1". After the samples are removed from the chamber through the load-lock apparatus, surface microanalysis is performed using diagnostics including atomic force microscopy (AFM), X-ray reflectivity (XRR), X-ray diffraction (XRD), Auger electron spectroscopy (AES), X-ray photoelectron spectroscopy (XPS), and scanning electron microscopy (SEM). These experiments are performed at the Center for Materials Microanalysis (CMM) at UIUC. They are used to measure changes in roughness, erosion, texture, and atomic composition. Six of the seven samples show marked increases in roughness, with the ML1 sample showing a decrease in roughness that may be due to a removal of the Ru capping layer to reveal a smoother Si surface. Increases in surface roughness leads to a decrease in sample reflectivity, especially in a grazing angle configuration. Total erosion of the samples is determined through use of SEM testing to be between 10 nm (Mo) and 54 nm (Au). AES reveals that various elements are deposited in the samples, including Xe, Mo, and W. More details can be found in Ref. [12].

### 3.4. Energy analyzer data

The direct fast ion debris field of the EUV source is characterized using the spherical sector energy analyzer described in Section 2. Details of these experiments are available elsewhere [8]. The results show that the species dominating the ion debris spectra are $Xe^{+}$ and $Xe^{2+}$, provided by the source fuel. Other measured ion species originate from the area around the pinch and include $Ar^{+}$, $Ni^{+}$, $Fe^{+}$, $Mo^{+}$, $W^{+}$, and $Si^{+}$. The amount of ion debris observed decreases as the buffer gas flow is increased, though some ion species show an increase with the initial addition of buffer gas. This relationship is illustrated by the data in Fig. 15, where the observed ion energy is 4 keV.

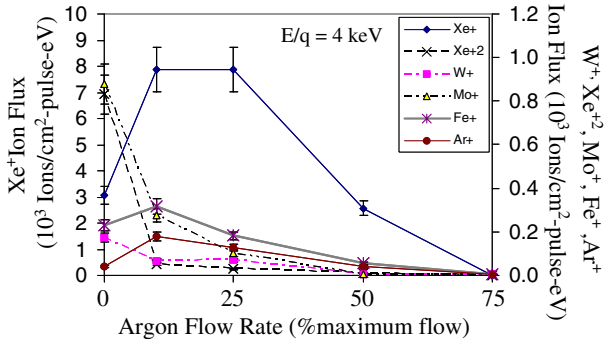


Fig. 15. Ion fluxes for $E = 4$ keV taken at 20° from centerline.

## 4. Conclusions

An experimental test chamber is created at the University of Illinois at Urbana-Champaign to conduct research relating to a commercially produced z-pinch EUV light source. The level of EUV energy emitted from the source is observed using the photodiode assembly discussed in Section 2. With this diagnostic, the data in Figs. 8 and 9 are obtained, showing that the pinch frequency has relatively little effect on the shot-to-shot energy output and that the addition of an argon gas curtain has a significant negative effect on the level of EUV energy measured at the photodiode. This problem is countered, however, by the positive effect of the gas curtain on debris mitigation. A trade-off must be made in this respect, though increasing the pumping speed in the main chamber is a solution that could improve the EUV signal while detracting from the debris mitigation capability to a lesser extent.

Also mounted on the test chamber is the Faraday cup assembly described in Section 2. The results of experiments using this diagnostic are presented in Figs. 10–12. With these data, the ion energy distributions of Fig. 13 are computed. Analysis of these plots shows that the maximum theoretical ion energy present is 53 keV, though further examination leads to the conclusion that the actual maximum value is likely to be lower.

Four positions are available inside the chamber in which samples are placed for exposure to the EUV light source at either a grazing or normal incidence angle. A rotatable photodiode array is used to take in situ reflectivity measurements of samples as they are exposed over time. A load-lock system is used to remove select sample holders while others continue to be exposed. Surface analysis of the first set of exposed samples shows increased roughness in most cases and erosion in all.

The chamber also allows for an array of experiments to be run in which the ion and neutral debris from the z-pinch is characterized and the angular variation observed. This is done using a Comstock AC-902B Spherical Sector Energy Analyzer [14] with a set of Burle Microchannel Plates [15], providing a basis for the evaluation of various mitigation schemes. Experiments confirm the presence of $Xe^{+}$ and $Xe^{2+}$ as the dominant ion species, while $Ar^{+}$, $Ni^{+}$, $Fe^{+}$, $Mo^{+}$, $W^{+}$, and $Si^{+}$ are also observed.

The issue of optics degradation inside a DPP EUV source is addressed by the XCEED experiment. The ESA diagnostic allows direct measurement of the erosive particle flux emitted by the pinch plasma so that time intensive sample exposures are not necessary for primary evaluation

of debris mitigation techniques. Once the efficacy of a method is evaluated, mirror samples are exposed under specifically chosen conditions to definitively evaluate the link between a debris mitigation technique and the amount by which it improves erosion. Cooperatively, the EUV photodiode is in place to monitor any trade-offs between debris mitigation and EUV output power. Experiments involving additional debris mitigation schemes are ongoing.

## Acknowledgments

This work performed at the University of Illinois at Urbana-Champaign is partially funded by International SEMATECH, Contract #308380 OF and Intel Components Research, Contract #SRA03-159, with assistance from XTREME Technologies GmbH. This research was partially carried out at the Center for Microanalysis of Materials at the University of Illinois, which is partially supported by the US Department of Energy under grant DEFG02-91-ER45439. The authors acknowledge XTREME Technologies GmbH and especially Dr. Tran Duc Chin for their expertise and support with the operation of the plasma source used. We thank the Theoretical and Applied Mechanics Machine shop and Electrical and Computer Engineering Machine Shop at the University of Illinois for the work they did on several elements of the experimental setup described here.

## References

[1] D.J. Resnick, W.J. Dauksher, D. Mancini, K.J. Nordquist, E. Ainley, K. Gehoski, J.H. Baker, T.C. Bailey, B.J. Choi, S. Johnson, S.V. Sreenivasan, J.G. Ekerdt, C.G. Willson, Proceedings of SPIE: Emerging Lithographic Technologies VI (2002) 205–213.

[2] U. Stamm, J. Kleinschmidt, K. Gäbel, H. Birner, I. Ahmad, D. Bolshukhin, J. Brudermann, T.D. Chin, F. Flohrer, S. Götze, G. Hergenhan, D. Klöpfel, V. Korobotchko, B. Mader, R. Müller, J. Ringling, G. Schriever, C. Ziener, Proceedings of SPIE: Emerging Lithographic Technologies VIII (2004) 133–144.

[3] XTREME Technologies GmbH, www.xtremetec.de, Gottingen, Germany.

[4] I.V. Fomenkov, W.N. Partlo, N.R. Böwering, A.I. Ershov, C.L. Rettig, R.M. Ness, I.R. Oliver, S.T. Melnychuk, O.V. Khodykin, J.R. Hoffman, V.B. Fleurov, J.M. Algots, J.W. Viatella, B.A.M. Hansson, O. Hemberg, A.N. Bykanov, E.A. Lopez, P.C. Oh, T.D. Steiger, D.W. Myers, Progress in Development of a High Power EUV Source for EUV Lithography, 2004. Available from: <http://www.sematech.org/resources/litho/meetings/euvl/20041105/04_Cymer_Update_Fomenkov.pdf>.

[5] J. Pankert, Philips's EUV Source: Main Messages, 2004. Available from: <http://www.sematech.org/resources/litho/meetings/euvl/20041105/08_Philips_Extreme_Update_Pankert.pdf>.

[6] U. Stamm, EUV Source Development at XTREME Technologies – An Update, 2004. Available from: <http://www.sematech.org/resources/litho/meetings/euvl/20041105/10_Xtreme_technologies_Update_Stamm.pdf>.

[7] M. McGeoch, PLEX EUV Source Update, 2004. Available from: <http://www.sematech.org/resources/litho/meetings/euvl/20041105/07_PLEX_LLC_Update_McGeoch.pdf>.

[8] E.L. Antonsen, K.C. Thompson, M.R. Hendricks, D.A. Alman, B.E. Jurczyk, D.N. Ruzic, Journal of Applied Physics (submitted for publication).

[9] U. Stamm, I. Ahmad, I. Balogh, H. Birner, D. Bolshukhin, J. Brudermann, S. Enke, F. Flohrer, K. Gäbel, S. Götze, G. Hergenhan, J. Kleinschmidt, D. Klöpfel, V. Korobotchko, J. Ringling, G. Schriever, C.D. Tran, C. Ziener, Proceedings of SPIE: Emerging Lithographic Technologies VII (2003) 119–129.

[10] L.A. Shmaenok, C.C. de Bruijn, H. Fledderus, R. Stuik, A.A. Schmidt, D.M. Simanovskii, A.A. Sorokin, T.A. Andreeva, F. Bijkerk, Proceedings of SPIE: Emerging Lithographic Technologies II (1998) 90–94.

[11] Kurt J. Lesker Company, Clairton, PA. Available from: <www.lesker.com>.

[12] H. Qiu, D.A. Alman, K.C. Thompson, J.B. Spencer, E.L. Antonsen, B.E. Jurczyk, D.N. Ruzic, T.P. Spila, Journal of Microlithography, Microfabrication, and Microsystems (submitted for publication).

[13] International Radiation Detectors Inc., Torrance, CA. Available from: <www.ird-inc.com>.

[14] Comstock Inc., Oak Ridge, TN. Available from: <www.comstockinc.com>.

[15] Burle Electro-Optics, Sturbridge, MA. Available from: <www.burle.com>.

[16] H. Meiling, V. Banine, P. Kürz, N. Harned, Proceedings of SPIE: Emerging Lithographic Technologies VIII (2004) 31–42.

[17] SPI Supplies, West Chester, PA. Available from: <www.2spi.com>.

[18] S. Bajt, H.N. Chapman, N. Nguyen, J. Alameda, J.C. Robinson, M. Malinowski, E. Gullikson, A. Aquila, C. Tarrio, S. Grantham, Proceedings of SPIE: Emerging Lithographic Technologies VII (2003) 236–248.